On the ecohydrology of structurally heterogeneous semiarid landscapes

Kelly K. Caylor,[1] Paolo D'Odorico,[2] and Ignacio Rodriguez-Iturbe[3]

Received 20 October 2005; revised 7 February 2006; accepted 27 March 2006; published 28 July 2006.

[1] Clarification of the coupled ecohydrological mechanisms that determine the spatial pattern and structural characteristics of vegetation in water-limited landscapes remains a vexing problem in both hydrological and vegetation sciences. A particular challenge is the fact that the spatial pattern of vegetation is both a cause and effect of variation in water availability in semiarid ecosystems. Here we develop a methodology to derive the landscape-scale distribution of water balance and soil moisture in a patchy vegetation mosaic based on the statistics of an underlying poisson distribution of individual tree canopies and their accompanying root systems. We consider the dynamics of water balance at a point to be dependent on the number of intersecting tree root systems and overlapping tree canopies. The coupling of individual pattern to landscape-scale distribution of soil water balance allows for investigations into the role of tree density, average canopy size, and the lateral extension of tree root systems on the spatiotemporal patterns of soil moisture dynamics, plant water uptake, and plant stress in a wide range of open woodland ecosystems. Our model is applied to southern African savannas, and we find that locations in the landscape that contain average vegetation structure correspond to conditions of minimum stress across a wide range of annual rainfall and vegetation densities. Furthermore, observed vegetation structural parameters are consistent with an optimization that simultaneously maximizes plant water uptake while minimizing plant water stress. Finally, the model predicts adaptive changes in the optimal lateral extent of plant roots which decreases with increasing rainfall along a regional gradient in mean annual precipitation.

Citation: Caylor, K. K., P. D'Odorico, and I. Rodriguez-Iturbe (2006), On the ecohydrology of structurally heterogeneous semiarid landscapes, *Water Resour. Res.*, *42*, W07424, doi:10.1029/2005WR004683.

1. Introduction

[2] The structure of terrestrial vegetation communities is strongly governed by the spatiotemporal distribution of growth-limiting resources [*Tilman*, 1988]. However, plants are not passive actors in this regard, and the biotic pattern of vegetation serves to redistribute key abiotic resources such as energy, water, and nutrients in important ways that are critical to the dynamics of the community through space and time. Therefore any theory regarding the structural configuration of plant communities must explicitly consider the consequences of spatial vegetation pattern on the dynamics of resource availability.

[3] Beginning with the analysis of spatial dynamics in tropical forests [*Denslow*, 1987], and continuing through the conceptualization of temperate [*Runkle and Yetter*, 1987] and boreal forest [*Bonan and Shugart*, 1989] community dynamics, it has become apparent that the nature of plant structural pattern and the dynamics of resource availability are highly interdependent [*Tilman and Kareiva*, 1997]. Although the forest community structure is often thought to be determined by prevailing resource conditions (i.e., climate or soil age), it is now recognized that the forest structure itself serves to modify resource availability. Perhaps best known is the paradigm of gap dynamics, by which species regeneration and subsequent patterns of canopy emergence occur within the localized patches of higher light availability formed by the death of a large canopy tree [*Shugart*, 1984].

[4] Regrettably, the incorporation of coupled abiotic and biotic determinants of resource availability into theories regarding the dynamics of semiarid ecosystems is not as well developed. Indeed, most initial approaches used to explain the particular nature of semiarid vegetation community structure relied exclusively on the role of external factors such as mean annual rainfall, or soil infertility imposed by geologic constraints. Within a regional context, these kinds of relationships often yield reasonable predictions of savanna ecosystem structure [*Sankaran et al.*, 2005; *Huxman et al.*, 2005]. However, it has also been recognized that the role of vegetation itself on resource availability can be critical in semiarid ecosystems [*Archer et al.*, 1988] and the strong control that individual plants can exert on local

[1]Department of Geography, Indiana University, Bloomington, Indiana, USA.
[2]Department of Environmental Sciences, University of Virginia, Charlottesville, Virginia, USA.
[3]Department of Civil and Environmental Engineering, Princeton University, Princeton, New Jersey, USA.

0043-1397/06/2005WR004683$09.00

Table 1. Location and General Characteristics of Four Kalahari Transect Landscapes

Site	Location		Rainfall,[a] mm/yr	Vegetation Characteristics	
	Latitude	Longitude		Vegetation Type	Percent Cover[b]
Tshane	−24.17	21.89	365	Open Acacia savanna	14
Ghanzi	−21.78	21.57	400	*Acacia-Terminalia* woodland	20
Pandamatenga	−18.66	25.50	698	Baikea woodland	40
Mongu	−15.44	23.25	879	Miombo woodland	65

[a]Annual rainfall from station data [*Scholes et al.*, 2002; *Williams and Albertson*, 2004].
[b]Percent woody vegetation determined from a combination of canopy mapping and densiometer measurements [*Caylor et al.*, 2003; *Scholes et al.*, 2002].

water balance is highlighted by the work of *Seyfried et al.* [2005], who find substantial variation in deep drainage under and between desert shrubs. Similarly, *Ludwig et al.* [2005] demonstrate the variation in surface moisture redistribution caused by the mosaic of vegetation patches and interpatch areas in many semiarid ecosystems. On the basis of these considerations, more recent spatial models of savanna structure have taken the spatial structure of semiarid ecosystems into account [*Jeltsch et al.*, 1999]. However, there remains a need to clarify the manner by which vegetation self-organizes within semiarid landscapes, and such clarification necessitates the development of conceptual models for spatial pattern formation in savanna (and similar dry woodland ecosystems). Research such as *Breshears and Barnes* [1999] represents a significant step forward toward a more unified conceptual model of interactions between plant pattern and soil moisture dynamics in savanna and other semiarid ecosystems.

[5] In our view, a significant challenge exists in coupling individual-scale patterns to landscape organization. Here we propose a simple model of soil moisture dynamics suitable for application to heterogeneous vegetation landscapes, such as those found in savannas or open woodlands. We are particularly interested in developing a framework that can generate hypotheses related to the causes and effects of horizontal variation in soil moisture arising from the patchy vegetation structure of individual tree canopies that is characteristic of many semiarid ecosystems. Although our presentation here focuses only on the effect of tree canopies on soil moisture dynamics, our approach is easily generalizable to the case of grass canopies only, or mixed tree-grass communities.

[6] The modeling framework developed in this study is applied to four landscapes in the Kalahari region of southern Africa. These landscapes represent individual study sites that span a regional gradient in average annual rainfall between about 300 mm/yr in southern Botswana to more than 900 mm/yr in western Zambia. Known as the Kalahari Transect, this south-north rainfall gradient is found on relatively uniform sandy soils [*Thomas and Shaw*, 1991], and therefore provides an excellent case study of coupled ecological and hydrological processes and their impact on the development of spatial patterns in vegetation and soil moisture. In the following sections, we will derive the landscape model and present model results based on parameters of landscape structure, soils, and climate for a series of savanna landscapes along the Kalahari transect. Site information on the vegetation and climate of these four sites is provided in Table 1.

2. Semiarid Vegetation Pattern

2.1. Poisson Distribution of Individual Trees

[7] In the simplest case, the spatial distribution of vegetation can be modeled as a homogeneous point process [*Batista and Maguire*, 1998] of overlapping vegetation canopies depicted in Figure 1a. The assumption that the spatial distribution of trees results from a homogeneous point process is here invoked only to develop an analytically tractable framework, even though it does not account for the aggregated tree distribution typically observed in savannas. Trees are represented as circles of random radius, r, drawn from an exponential distribution with mean μ_r. Tree centers are modeled as a 2-D Poisson process of rate λ_t, where λ_t represents the mean number of centers per unit area. Thus the number, n_C, of canopies occurring at a

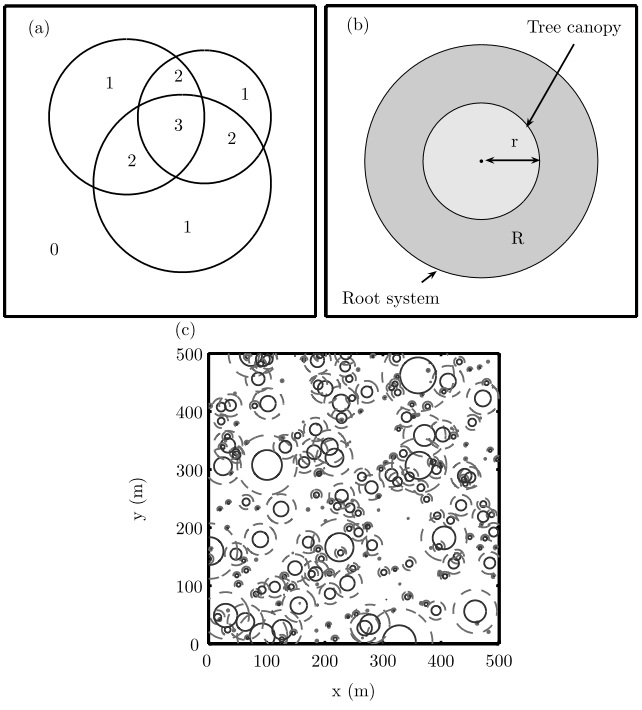

Figure 1. (a) Schematic of the 2-D Poisson model, indicating the number of overlapping canopies in each portion of the landscape; (b) depiction of a single tree's canopy (light shading) and its accompanying root system (dark shading), where r is the canopy radius and R is the root system radius such that $a_t = R/r$; (c) a representative landscape, including tree canopies (solid lines) and root system distributions (dashed lines).

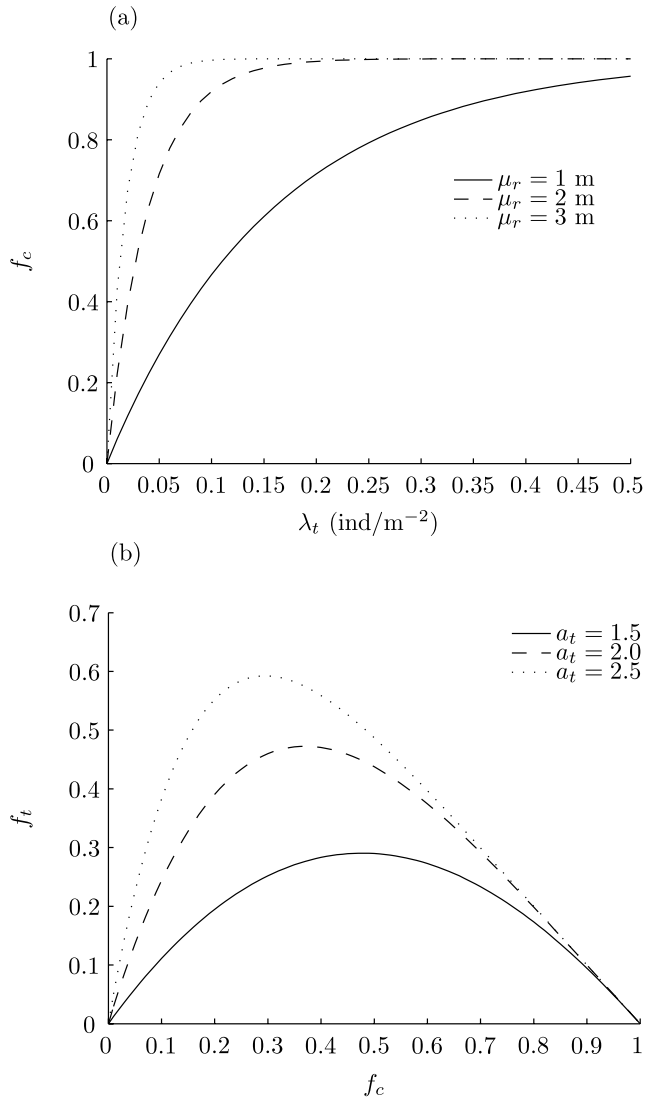

Figure 2. (a) Dependence of fractional cover, f_c, on density, λ_t (ind/m^2), and expected tree radius, μ_r (meters). (b) Dependence of the region of bare soil exploited by canopy roots, f_t, on f_c and the ratio of root radii to tree radii, a_t.

randomly chosen point (Figure 1a) has a Poisson distribution [*Cox and Miller*, 1965] of mean $\langle n_C \rangle = \lambda_t \mu_A$, where $\mu_A = 2\pi\mu_r^2$ is the expected area of an individual tree canopy. The probability of having no trees at a given point is

$$P[n_C = 0] = e^{-2\pi\lambda_t\mu_r^2} \tag{1}$$

while the fractional canopy cover, f_c, is given by

$$f_c = 1 - P[n_C = 0] = 1 - e^{-2\pi\lambda_t\mu_r^2}. \tag{2}$$

[8] From equation (2) it is clear that the specification of λ_t and μ_r completely determines the particular landscape configuration. The resulting relationship between the parameter λ_t of the Poisson process, the cover fraction, f_c, and the average tree radius, μ_r, are shown in Figure 2a.

[9] In this study we are interested in the interactions between tree canopies, their accompanying root systems, and their effect on the overall dynamics of soil moisture. Therefore we extend the basic framework presented in equation (2) to calculate the fraction of bare soil area invaded by tree roots. Accordingly, we define $a_t = \mu_R/\mu_r$, which is the ratio between root and canopy radii as shown in Figure 1b. The value of a_t is taken to be a fixed property of the vegetation in each landscape. From this definition we can determine the fraction of soil not covered by roots according to

$$f_{b_R} = e^{-2\pi\lambda_t a_t^2 \mu_r^2} = (1 - f_c)^{a_t^2}. \tag{3}$$

Finally, we also consider the fraction, f_t, of soil invaded by the roots outside the vertical projection of the canopy when $a_t \geq 1$, which corresponds to the gray dotted region in Figure 1b. This value is given by

$$f_t = 1 - f_c - f_{b_R} = (1 - f_c) - (1 - f_c)^{a_t^2}. \tag{4}$$

[10] The resulting relationship between the cover fraction, f_c, and the fraction of soil invaded by roots, f_t, are shown in Figure 2b. The distribution of trees and roots resulting from the Poisson process (Figure 1c) is used to study the effect of vegetation on the spatial patterns of soil moisture, which determines the occurrence and severity of water stress in semiarid vegetation. This approach makes it possible to mechanistically investigate the relation between vegetation patterns and the distribution of soil moisture, components of water balance, and the occurrence of plant water stress. Table 2 provides parameters of vegetation structure for the four study landscapes. Tree density, λ_t increases across the transect from south (Tshane) to north (Mongu), as does average tree size, μ_r.

[11] The values of tree density and tree size in Table 2 are taken from the same field sites in Table 1 where percent woody cover was determined using mapping and densiometer techniques. However, we note that there are slight disagreements between the observed percent woody cover in Table 1 and that predicted by the values of λ_t and μ_r within a Poisson landscape (Table 2), particularly at sites with intermediate rainfall. This discrepancy is due to the tendency for vegetation to form aggregated patterns in many

Table 2. Site-Specific Rainfall and Vegetation Structure Parameters Used in the Landscape Soil Moisture Model

	Rainfall[a]		Vegetation Structure[b]		
Site	λ, day^{-1}	α, mm	λ_t, ind/m^2	μ_r, m	Percent Cover[c]
Tshane	0.150	10	0.018	1.62	17
Ghanzi[d]	0.175	10	0.030	1.65	27
Pandamatenga	0.290	10	0.043	1.70	37
Mongu	0.380	10	0.091	1.85	65

[a]Rainfall parameters taken from the presentation of *Porporato et al.* [2003].
[b]Vegetation parameters from *Caylor et al.* [2003].
[c]Percent cover values determined using λ_t, μ_r, and equation (2).
[d]Ghanzi vegetation data from unpublished field observations (K. K. Caylor, 2005).

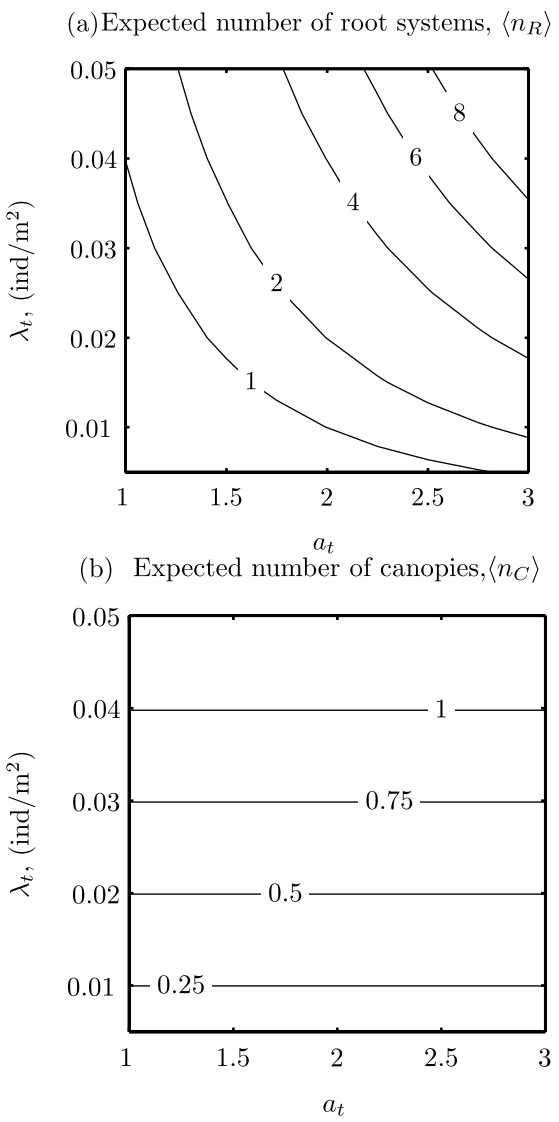

Figure 3. Expected number of (a) landscape-scale root systems and (b) tree canopies for a range of densities, λ_t (ind/m^2), and rooting ratios, a_t, given a constant average tree radius, μ_r = 2 m. The expected number of root system intersections depends on both canopy density and rooting ratio, while the expected number of canopy intersections only depends on tree density.

savanna landscapes [*Caylor et al.*, 2003], which our current model does not address. An extension of our approach would be to investigate the degree of spatial clumping on landscape soil moisture within the framework we provide. However, our focus here remains the simplest possible description of vegetation structure, i.e., a null model of spatially random vegetation distribution.

2.2. A Spatially Distributed Landscape Model

[12] A theoretical framework is developed for estimating landscape-scale soil moisture variation using the joint distribution of tree canopies and tree roots within a semiarid landscape. Under the assumption that trees are distributed randomly according to a 2-D Poisson process and have radii drawn from an exponential distribution with mean radius μ_r, we noted above that the distribution of canopy overlaps follows a Poisson distribution, with an average number of canopy overlaps,

$$\langle n_C \rangle = 2\pi\mu_r^2\lambda_t. \tag{5}$$

[13] Additionally, it follows from our earlier discussion that the expected number of overlappings of root systems is

$$\langle n_R \rangle = 2\pi(\mu_r a_t)^2\lambda_t, \tag{6}$$

where a_t is the fixed ratio of root radius to canopy radius, which we defined previously. Figure 3 depicts the expected number of canopies and root systems at a point for landscapes corresponding to a range of densities, λ_t, and root ratios, a_t, with constant average canopy radius, μ_r = 2 meters.

[14] The probability of finding a location in the landscape with n_R overlapping root systems and n_C overlapping canopies is the joint distribution of n_R and n_C, notated as $P(n_R \cap n_C)$. Under the condition that the specified ratio of root to canopy areas is set to be one (i.e., $a_t = 1$) so that all root systems are exactly the same size as all canopy areas, it is apparent that $P(n_R \cap n_C) = P(n_R) = P(n_C)$, since each root system is overlain by a single canopy area with probability 1. However, when the specified value of $a_t \neq 1$, the joint probability distribution of n_R and n_C is derived as

$$P(n_R \cap n_C)\begin{cases} P(n_R|n_C)P(n_C), & \text{if } a_t < 1 \\ P(n_C|n_R)P(n_R), & \text{if } a_t > 1 \end{cases} \tag{7}$$

where $P(n_C|n_R)$ and $P(n_R|n_C)$ are the conditional probability of n_C on n_R and viceversa respectively, while $P(n_C)$ and $P(n_R)$ are Poisson distributions with mean values of $\langle n_C \rangle$ and $\langle n_R \rangle$, as described above. The derivation of the conditional probabilities for $P(n_C|n_R)$ and $P(n_R|n_C)$ proceed in a similar manner. Here we focus on $P(n_C|n_R)$, which is determined for cases where root systems are always larger than canopy areas (i.e., $a_t \geq 1$), the most likely condition for the kinds of semiarid ecosystems considered here. Following the approach presented in the Appendix, we define the quantity $\tau = 1/a_t^2$, and find that the general form of the conditional probability $P(n_C|n_R)$ is a binomial distribution with mean $n_R\tau$ and variance $n_R\tau(1 - \tau)$ so that

$$P(n_C|n_R) = \binom{n_R}{n_C}\tau^{n_C}(1-\tau)^{(n_R-n_C)} \quad (n_C = 0, 1, ..., n_R), \tag{8}$$

where

$$\binom{n_R}{n_C} = \frac{n_R!}{n_C!(n_R - n_C)!} \tag{9}$$

is the binomial coefficient. The expression of $P(n_C|n_R)$ in equation (8) is now used to calculate $P(n_C \cap n_R)$ using equation (7), given that $P(n_R)$ is the Poisson distribution of the number of root system occurrences given by

$$P(n_R) = \frac{\left(2\lambda_t\pi\mu_r^2a_t^2\right)^{n_R}e^{-2\lambda_t\pi\mu_r^2a_t^2}}{n_R!} \qquad (n_R = 0, 1, ...). \tag{10}$$

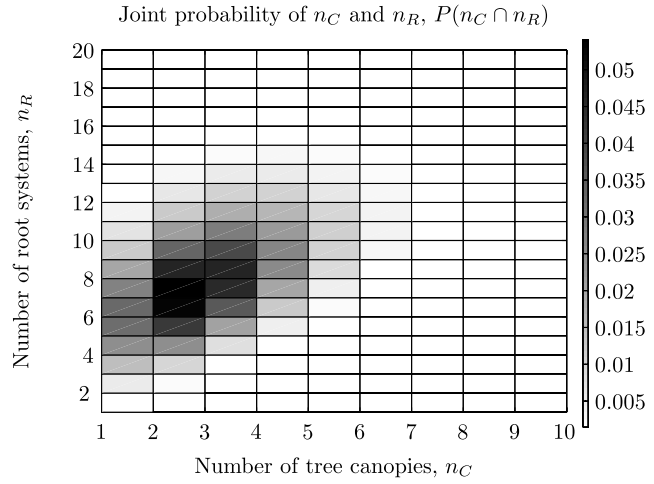

Figure 4. Joint distribution of canopy and root systems, $P(n_C \cap n_R)$, for the case $\lambda_t = 0.05$ ind/m^2, $\mu_r = 2$ m, and $a_t = 2$. Because $a_t > 1$, overlapping root systems are more frequent than overlapping tree canopies.

[15] Figure 4 provides the joint distribution of canopies and roots according to equation (7) with $\lambda_t = 0.05$, $\mu_r = 2$ meters, and $a_t = 2$. Having derived and verified the distribution $P(n_C \cap n_R)$, it is now necessary to connect the distribution of canopies and root systems in the landscape to the soil moisture dynamics which occur therein.

3. Probabilistic Soil Moisture

[16] Following the presentations of *Laio et al.* [2001] and *Rodriguez-Iturbe et al.* [1999b], we characterize the daily soil moisture balance according to the stochastic arrival of rainfall events and the rate of soil moisture losses from the active soil given by

$$nZ_r \frac{\mathrm{d}s(t)}{\mathrm{d}t} = \vartheta[s(t);t] - \chi[s(t)], \tag{11}$$

where n is the soil porosity, Z_r is the depth of the active soil layer, and $s(t)$ is the relative soil moisture content ($0 \leq s(t) \leq 1$). The term $\vartheta[s(t); t]$ is the stochastic portion of the soil moisture balance, and represents the amount of rainfall that infiltrates the soil column which is rainfall, $R(t)$, less the sum of interception, $I(t)$ and the rate of runoff, $Q[s(t); t]$. The deterministic loss function $\chi[s(t)]$ includes evaporation, $E[s(t)]$, transpiration, $T[s(t)]$, and vertical drainage $L[s(t)]$, out the bottom of the active soil layer.

3.1. Rainfall and Interception

[17] Rainfall, $R(t)$, is modeled as a marked Poisson process of storm arrivals at rate λ (day^{-1}), with each storm having a random depth, d, that is exponentially distributed with mean α (mm). Interception, $I(t)$, is the amount of rainfall, Δ (mm), that does not reach the soil surface due to canopy storage, and is accounted for by modifying the rate of storm occurrence ($\lambda' = \lambda e^{-\Delta/\alpha}$) for locations with canopies [*Rodriguez-Iturbe et al.*, 1999a]. We use an empirical estimation of canopy interception given by

$$\Delta = LAI_C \times h \times n_C, \tag{12}$$

where LAI_C is the leaf area index of vegetation canopies (Table 3), and h is a characteristic amount of interception per unit leaf area which we take to be equal to .2 mm [*Scholes and Walker*, 1993]. In this way, although we consider rainfall to be a spatially homogenous processes within the landscape, we note that interception (and subsequent infiltration) rates vary according to the number of canopies (n_C) present at each location within the landscape. Whenever rainfall depth exceeds the storage capacity (nZ_r) of the rooting layer, we assume that the excess is converted to surface runoff. Runoff does not play a significant role in this study, as both infiltration-excess runoff and saturation-excess overland flow seldom occur, due to the presence of deep sandy soils with relatively high infiltration capacity and deep water tables.

3.2. Effect of Canopies and Roots on Evapotranspiration

[18] Our goal is to determine the distribution of soil moisture, rates of evaporation, plant water uptake, and plant water stress within a structurally heterogeneous landscape of tree canopies and their accompanying root systems. Therefore we formulate representations of evaporation and plant water uptake governed by n_C and n_R. In particular, we recognize that the parameter n_R determines the local rate of soil water uptake, while n_C controls the evaporative loss of soil moisture and regulates the partitioning of evapotranspiration into soil evaporation and plant water uptake. The vertical root profile is here assumed to be uniform and individual plant root uptake is evenly partitioned throughout the thickness of the soil layer, Z_r. We assume that canopies reduce energy available for evaporation due to shading effects according to an exponential distribution (e.g., Beer's law), such that

$$\phi_E(n_C) = e^{-kn_C} \tag{13}$$

where ϕ_E is the fraction of incoming energy available for bare soil evaporation under n_C canopies and k is an extinction coefficient of evaporative demand that we take to be equal to 0.35 [*Brutsaert*, 1982]. The number, n_C, of overlying canopies determines the fraction, $1 - \phi_E$, of net solar irradiance intercepted and therefore available for transpiration from the plant stomata.

[19] Because root water uptake depends on the amount of energy incident on each root system's corresponding canopy, we must recognize that plant water extraction rate from the soil is constrained by the total energy absorbed by

Table 3. Parameters Used in the Landscape Soil Moisture Model and Their Sources

Parameter	Value	Source
PET	6 mm/d	*Bahlotra* [1987]
LAI_C	2.0 m^2/m^2	*Williams and Albertson* [2004]
K_s	2000 mm/d	*Williams and Albertson* [2004]
Zr	600 mm	*Hipondoka et al.* [2003]
s^*	0.275	*Williams and Albertson* [2004]
s_{wilt}	0.125	*Williams and Albertson* [2004]
s_h	0.04	*Porporato et al.* [2003]
s_{fc}	0.35	*Porporato et al.* [2003]
β	12.5	*Laio et al.* [2001]
n	0.40	*Williams and Albertson* [2004]

individual plant canopies. To accommodate the role that canopy light interception plays in determining root water uptake, we use equation (13) to estimate the amount of fractional energy absorption per canopy (φ) for n_C cooccurring canopies, which we denote as

$$\varphi = \frac{1 - \phi_E(n_C)}{n_C}. \tag{14}$$

[20] In order to estimate individual water uptake rates for n_R separate overlapping root systems, it would be necessary to know φ for each canopy associated with each root system. However, given our statistical description of the landscape, it is apparent that root systems existing at a certain point can belong to trees whose canopies have no shading effect on the same point. Therefore the exact value of φ for the canopy associated with a particular root system at a random location within the landscape is unknown in our modeling framework. In the absence of specific values of φ for each location in the landscape, we can instead determine the expected amount of energy absorbed per canopy, $\overline{\varphi}$, which we use to constrain water uptake per root system. The expected fraction of energy absorbed per canopy is determined according to the expected value of n_C at locations where canopies are present and is given by

$$\overline{\varphi} = \sum_{n_C=1}^{\infty} \left(\frac{1 - \phi_E(n_C)}{n_C} \right) P_1(n_C), \tag{15}$$

where $P_1(n_C)$ is the Poisson distribution of the number of canopies renormalized for the range $n_C \geq 1$ according to

$$P_1(n_C) = \frac{P(n_C = 1...\infty)}{1 - P(n_C = 0)}. \tag{16}$$

[21] Recognizing that each root system is associated with a single tree canopy, we use equation (15) as a measure of the energetic constraint on root uptake demand per canopy. Therefore we approximate the fraction of potential water uptake that takes place at a location containing n_R root systems (connected to n_R separate canopies) according to

$$\phi_T(n_R) = \overline{\varphi} \cdot n_R. \tag{17}$$

3.3. Soil Moisture Loss Function

[22] The values of $\phi_E(n_C)$ and $\phi_T(n_R)$ determine the relative amounts of evaporation and plant water uptake at a location with n_C canopies and n_R root systems. At any given location, the sum of evaporation and plant water uptake may exceed the potential evapotranspiration rate (PET mm/day). This is particularly true in open areas that contain many root systems under conditions of high water availability. However, the potential evapotranspiration rate does provide an upper bound on the landscape average evapotranspiration. In addition, the rate of evaporation and plant water uptake both depend on the available soil moisture at any given time. To accommodate the role of soil moisture limitation on evaporation, we assume that evaporation linearly increases from zero at the soil hygroscopic point, s_h, to a maximum evaporation rate, $\phi_E(n_C) \times$ PET, at field capacity, s_{fc}. Similarly, we assume that water uptake from roots (i.e., transpiration) exhibits a linear response to soil moisture availability, increasing from zero at the plant wilting point, s_w, to the maximum, $\phi_T(n_R) \times$ PET, at the point of incipient stomatal closure, s^*. At soil moisture values above s^*, water uptake proceeds at the maximum rate, just as evaporation proceeds at the maximum rate above field capacity. Finally, above field capacity, we consider leakage loss from the lower boundary of the soil layer. Here we determine leakage according to *Laio et al.* [2001], based on the saturated hydraulic conductivity, K_s (mm/day), and on the soil water content as given by

$$L(s) = K_s \frac{e^{\beta(s - s_{fc})} - 1}{e^{\beta(1 - s_{fc})} - 1}, \qquad \left(\text{if } s > s_{fc}, \text{ else } L(s) = 0\right), \tag{18}$$

with β being a parameter (see Table 3) dependent on soil texture [*Laio et al.*, 2001].

[23] The overall loss function, $\rho(s)$, due to evaporation, uptake, and leakage is a piecewise continuous function increasing from zero at the hygroscopic point (s_h) to a maximum rate of soil water loss through evaporation and root uptake which occurs at field capacity (s_{fc}). Above field capacity, nonlinear leakage effects begin to dominate the rate of water loss from the soil layer. The complete form of the loss function is given by

$$\rho(s) = \frac{\chi(s)}{nZ_r} = \frac{E(s) + T(s) + L(s)}{nZ_r}$$

$$= \begin{cases} 0, & 0s \leq s_h, \\ \eta_e \dfrac{s - s_h}{s_{fc} - s_h}, & s_h < s \leq s_w, \\ \eta_e \dfrac{s - s_h}{s_{fc} - s_h} + \eta_t \dfrac{s - s_w}{s^* - s_w}, & s_w < s \leq s^*, , \\ \eta_e \dfrac{s - s_h}{s_{fc} - s_h} + \eta_t, & s^* < s \leq s_{fc}, \\ \eta_e + \eta_t + m\left(e^{\beta(s - s_{fc})} - 1\right), & s_{fc} < s \leq 1, \end{cases} \tag{19}$$

where

$$\eta_e = \phi_E(n_C) \times \frac{PET}{nZ_r}, \tag{20}$$

$$\eta_t = \phi_T(n_R) \times \frac{PET}{nZ_r}, \tag{21}$$

and

$$m = \frac{K_s}{nZ_r\left(e^{\beta(1 - s_{fc})} - 1\right)}. \tag{22}$$

3.4. Probability Distribution of Soil Moisture at a Point

[24] From the previous sections, we can define the soil water balance through a stochastic differential equation (equation (11)) with a deterministic loss function (equation (19)) depending on the number of canopies (n_C) and

roots (n_R). The solution of this stochastic differential equation proceeds in the same manner as by *Laio et al.* [2001], and yields the steady state probability distribution of relative soil moisture:

$$p(s) = \begin{cases} e^{-\gamma s}(s - s_h)^{\frac{\lambda'(s_{fc}-s_h)}{\eta_e}-1} & s_h < s \le s_w, \\ C_2 \times e^{-\gamma s}\left((s - s_h)(s^* - s_w)\eta_e + (s_{fc} - s_h)(s - s_w)\eta_t\right)^{\varepsilon-1} & s_w < s \le s^*, \\ C_3 \times e^{-\gamma s}\left(s\eta_e + s_{fc}\eta_t - s_h(\eta_e + \eta_t)\right)^{\frac{\lambda'(s_{fc}-s_h)}{\eta_e}-1} & s^* < s \le s_{fc}, \\ C_4 \times e^{\frac{(\lambda'-\gamma\omega)s}{\omega}}\left(\eta_e + \eta_t + m\left(e^{\beta(s-s_{fc})} - 1\right)\right)^{\frac{\lambda'}{\beta\omega}-1} & s_{fc} < s \le 1. \end{cases} \quad (23)$$

[25] The terms C_2, C_3, and C_4 in equation (23) are given by

$$C_2 = (s_w - s_h)^{\frac{\lambda'(s_{fc}-s_h)}{\eta_e}-1}(\eta_e(s^* - s_w)(s_w - s_h))^{1-\varepsilon}, \quad (24)$$

$$C_3 = C_2 \times \left(\eta_e(s^* - s_h)(s^* - s_w) + \eta_t(s_{fc} - s_h)(s^* - s_w)\right)^{\varepsilon-1} \times \left(s^*\eta_e + s_{fc}\eta_t - s_h(\eta_e + \eta_t)\right)^{1-\frac{\lambda'(s_{fc}-s_h)}{\eta_e}}, \quad (25)$$

$$C_4 = C_3 \times e^{-\gamma s_{fc} - \frac{s_{fc}(\lambda'-\gamma\omega)}{\omega}}(\eta_e + \eta_t)^{\frac{\lambda'}{\beta\omega}+1} \times \left(s_{fc}(\eta_e + \eta_t) - s_h(\eta_e + \eta_t)\right)^{\frac{\lambda'(s_{fc}-s_h)}{\eta_e}-1}. \quad (26)$$

[26] Finally, the terms ε and ω in the above equations are defined as

$$\varepsilon = \frac{\lambda'(s_{fc} - s_h)(s_t - s_w)}{\eta_e(s^* - s_w) + \eta_t(s_{fc} - s_h)}, \quad (27)$$

and

$$\omega = \eta_e + \eta_t - m. \quad (28)$$

[27] Figure 5 demonstrates some examples of steady state probability distributions of relative soil moisture in both bare and vegetated areas along the Kalahari transect. As expected, the model predicts increased soil moisture values in bare locations (with neither roots or canopies) as rainfall rates increase from Tshane (dry) to Mongu (wet), according to Table 1. However, the presence of average vegetation structure (i.e., $n_C = \langle n_C \rangle$ & $n_R = \langle n_R \rangle$) in each landscape leads to a much reduced distribution of relative soil moisture especially in the most northern site. Furthermore, the increase of vegetation density and size across the rainfall gradient (Table 2) closely matches the increase in rainfall. It is this combination of increasing rainfall rates and increasing vegetation density that leads to similar predictions of soil moisture conditions across the rainfall gradient. The results suggest that across the transect, increases in resource availability are matched by increases in resource exploitation by the vegetation. Viewed in this manner, the density and size of vegetation may be seen to represent a structural configuration that maintains the soil moisture distribution at a level that is just above a critical stress threshold. In the following section we examine the patterns of landscape average water balance across the four study sites.

4. Landscape Average Water Balance

[28] For a given location with n_C canopies and n_R root systems, we use the steady state probability of relative soil moisture, $p(s)$, defined in the previous section, to determine average values of the water balance,

$$\langle R(n_C, n_R)\rangle = \langle E(n_C, n_R)\rangle + \langle T(n_C, n_R)\rangle + \langle L(n_C, n_R)\rangle \quad (29)$$

where $\langle R(n_C, n_R)\rangle$ is the average rainfall rate (mm/day), and $\langle E(n_C, n_R)\rangle$, $\langle T(n_C, n_R)\rangle$, and $\langle L(n_C, n_R)\rangle$ are the steady state average rates of evaporation, root water uptake (i.e., transpiration), and leakage respectively (mm/day). These quantities are given by

$$\langle R(n_C, n_R)\rangle = \alpha \times \lambda' \quad (30)$$

$$\langle E(n_C, n_R)\rangle = \eta_e \times nZ_r \times \int_{s_h}^{s_{fc}} \frac{s - s_h}{s_{fc} - s_h} p(s)\mathrm{d}s \quad (31)$$

$$\langle T(n_C, n_R)\rangle = \eta_t \times nZ_r \times \left(\int_{s_w}^{s^*} \frac{s - s_w}{s^* - s_w} p(s)\mathrm{d}s + \int_{s_{fc}}^{1} p(s)\mathrm{d}s\right) \quad (32)$$

$$\langle L(n_C, n_R)\rangle = m \times nZ_r \times \int_{s_{fc}}^{1} \left(e^{\beta(s-s_{fc})} - 1\right) p(s)\mathrm{d}s. \quad (33)$$

[29] The landscape averages of soil moisture, $\overline{\langle s\rangle}$, transpiration, $\overline{\langle t\rangle}$, evaporation, $\overline{\langle E\rangle}$, and leakage loss, $\overline{\langle L\rangle}$,

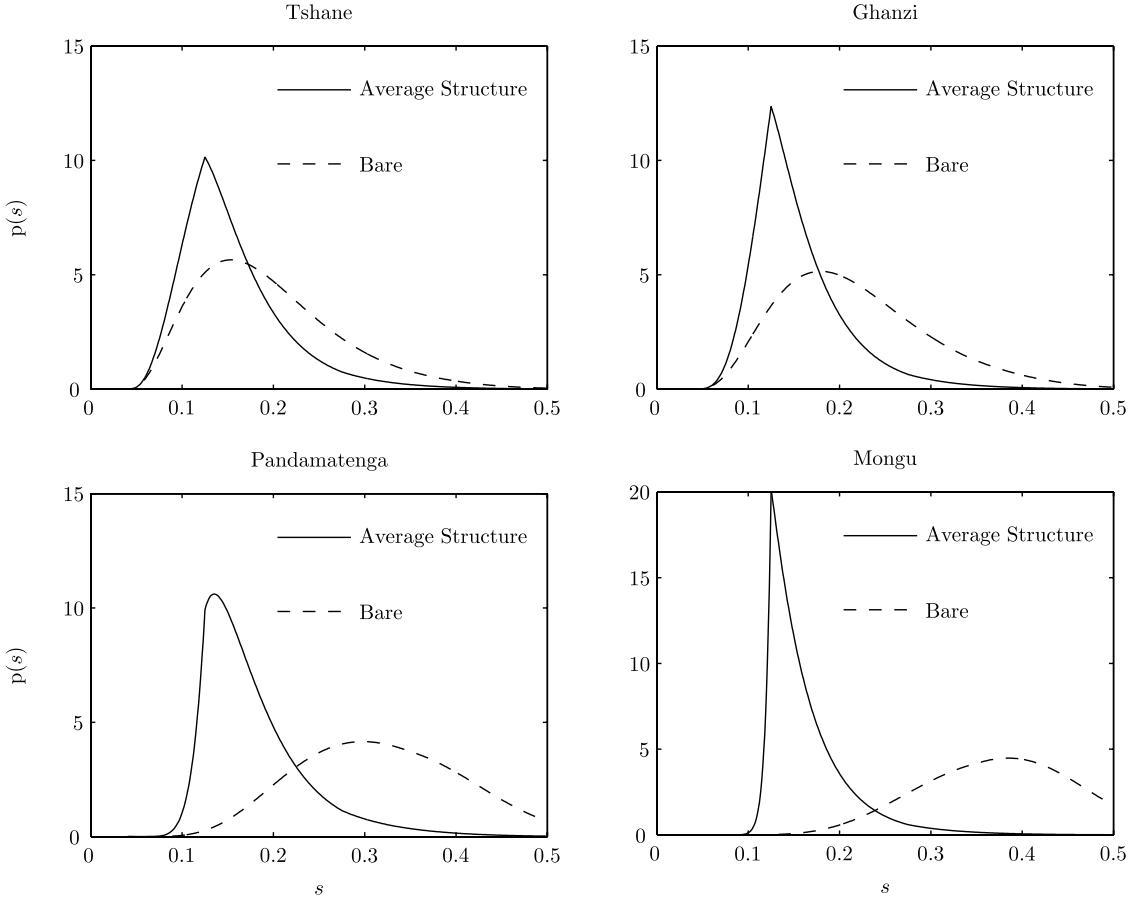

Figure 5. Probability distribution, $p(s)$, of relative soil moisture for a point containing the average vegetation structure (solid lines) and bare soil (dashed lines) within four Kalahari landscapes. Model parameters are provided in Tables 2 and 3. The value of a_t is assumed to be 2 in all four landscapes. In the absence of any canopies or roots the average relative soil moisture increases across the four landscapes with increasing rainfall from Tshane to Mongu. However, the average number of overlapping canopies and root areas also increases with greater values of tree density and average tree size (Table 2 and Figure 3). The result is similar distributions of relative soil moisture for locations with average vegetation structure in each landscape across the rainfall gradient.

depend on the joint distribution of canopies and roots, $P(n_C \cap n_R)$ according to

$$\overline{\langle s \rangle} = \sum_{n_C, n_R} P(n_C \cap n_R) \langle s(n_C, n_R) \rangle, \tag{34}$$

$$\overline{\langle E \rangle} = \sum_{n_C, n_R} P(n_C \cap n_R) \langle E(n_C, n_R) \rangle, \tag{35}$$

$$\overline{\langle T \rangle} = \sum_{n_C, n_R} P(n_C \cap n_R) \langle T(n_C, n_R) \rangle, \tag{36}$$

$$\overline{\langle L \rangle} = \sum_{n_C, n_R} P(n_C \cap n_R) \langle L(n_C, n_R) \rangle. \tag{37}$$

[30] Figure 6 shows the relative contributions of evaporation, transpiration, and leakage to the soil moisture losses in different landscapes across the Kalahari transect. In this analysis, the rainfall, tree density and canopy size parameters are those measured in the field, while the value of a_t is assumed equal to 2 in each landscape. As expected, due to the dry soil moisture conditions, leakage is negligible in all landscapes, while the relative importance of transpiration increases (with respect to evaporation) in the south-to-north direction due to the presence of denser canopies (see Table 2). We now turn to measures of plant water stress and the degree to which vegetation structural patterns in Kalahari landscapes are coorganized around resource use and stress avoidance.

5. Plant Water Stress and Stress-Weighted Plant Water Uptake

[31] At each location in a landscape containing n_C canopies and n_R roots, we consider the water stress distribution according to the frequency and magnitude of excursions of the relative soil moisture below the critical value of s^* that corresponds to the point at which plants begin to close their stomata. *Porporato et al.* [2001] review the physiological impacts of reduced water variability on plant performance and the onset of plant water stress. In order to account for

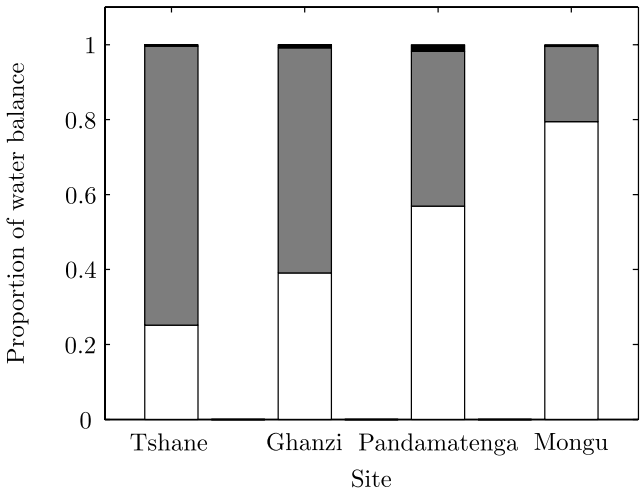

Figure 6. Model predictions of the relative contribution of plant water uptake (white bars), evaporation (gray bars), and leakage (black bars) to the average water balance of four landscapes within the Kalahari region of southern Africa. Annual rainfall increases from an average of 365 mm/yr at Tshane to 850 mm/yr at Mongu. Model parameters are provided in Tables 2 and 3, and a_t is assumed to be equal to 2 in each landscape.

the effects of increasing soil moisture deficit on plant physiological performance, we adopt the water stress formulation first proposed by *Rodriguez-Iturbe et al.* [1999a], which determines plant water stress, ξ, according to

$$\xi(s) = \begin{cases} 1 & s \le s_w \\ \left(\frac{s^* - s}{s^* - s_w}\right)^q & s_w < s \le s^*, \\ 0 & s > s^*, \end{cases} \tag{38}$$

where q is a measure of nonlinearity in the relationship between relative soil moisture deficit and plant stress response, here taken to be equal to 2 following the discussion of *Porporato et al.* [2001].

5.1. Stress-Weighted Plant Water Uptake

[32] Any measure of "optimal" conditions for plant water use must appropriately balance maximization of resource use with minimization of stress occurrence. For example, as the average root ratio (a_t) increases, an individual plant may be able to increase its plant water uptake rate. However, the increased number of overlapping roots associated with an increase in plant root ratio (Figure 3), leads to higher landscape average uptake rates and more rapid onset of stress conditions whenever water becomes limiting. To relate these conditions to the soil and vegetation parameters, we define an average stress-weighted plant water uptake, $\langle\zeta\rangle$, as the product of the average plant water uptake rate, $\langle T\rangle$, and the complement of the average plant water stress, $1 - \langle\xi\rangle$, so that

$$\langle\zeta\rangle = \langle T\rangle[1 - \langle\xi\rangle], \tag{39}$$

where $\langle\zeta\rangle$ takes units of mm/day. This formulation of $\langle\zeta\rangle$ reflects the principle that resources obtained under stressed conditions have a greater cost (and therefore less value) than resources obtained under stress-free conditions. As average stress increases at a given average water uptake level, the value of the resulting average stress-weighted plant water uptake decreases.

[33] In each landscape, there is a large degree of structural heterogeneity from point to point within the landscape; we seek to understand how plant water stress and rates of plant water uptake vary within the landscape at various locations representing a range of vegetation structural configurations. We define three characteristic vegetation structures that can be compared across each of the four study landscapes. The first is an "open" location, where the number of canopies is zero, and the number of roots present is simply the landscape average number of roots, so that $n_C = 0$ and $n_R = \langle n_R\rangle$. The second location is an average location, where $n_C = \langle n_C\rangle$ and $n_R = \langle n_R\rangle$ and the third is an "above average" location, where $n_C = 2\langle n_C\rangle$ and $n_R = 2\langle n_R\rangle$.

[34] The effect of each of these vegetation structural configurations on steady state average stress is shown in Figure 7. In each landscape, locations with an "average" vegetation structure correspond to points in the landscape that exhibit a lower amount of stress than locations with either less vegetation structure or points with greater densities of roots and canopies. Because canopies reduce soil evaporation rates (see equation (13)), locations with few canopies (i.e., "open" areas in Figure 7) correspond to locations with high rates of evaporation. These areas experience rapid depletion of soil moisture after rainfall events. In contrast, locations with a large number of canopies and

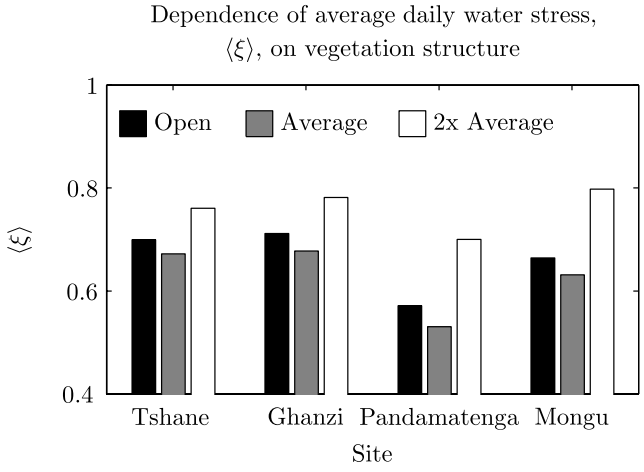

Figure 7. Steady state average values of the daily relative plant stress, $\langle\xi\rangle$, for locations containing three different structural configurations in four Kalahari landscapes. Mean annual rainfall increases from Tshane to Mongu according to Table 1. Model paramaters taken from Tables 2 and 3. Black bars indicate stress conditions at an open location (no canopies); gray bars indicate locations with an average number of canopies and roots, and white bars indicate a location with twice the average number of canopies and roots within each landscape. Across all landscapes, locations with the average structure exhibit the lowest average stress.

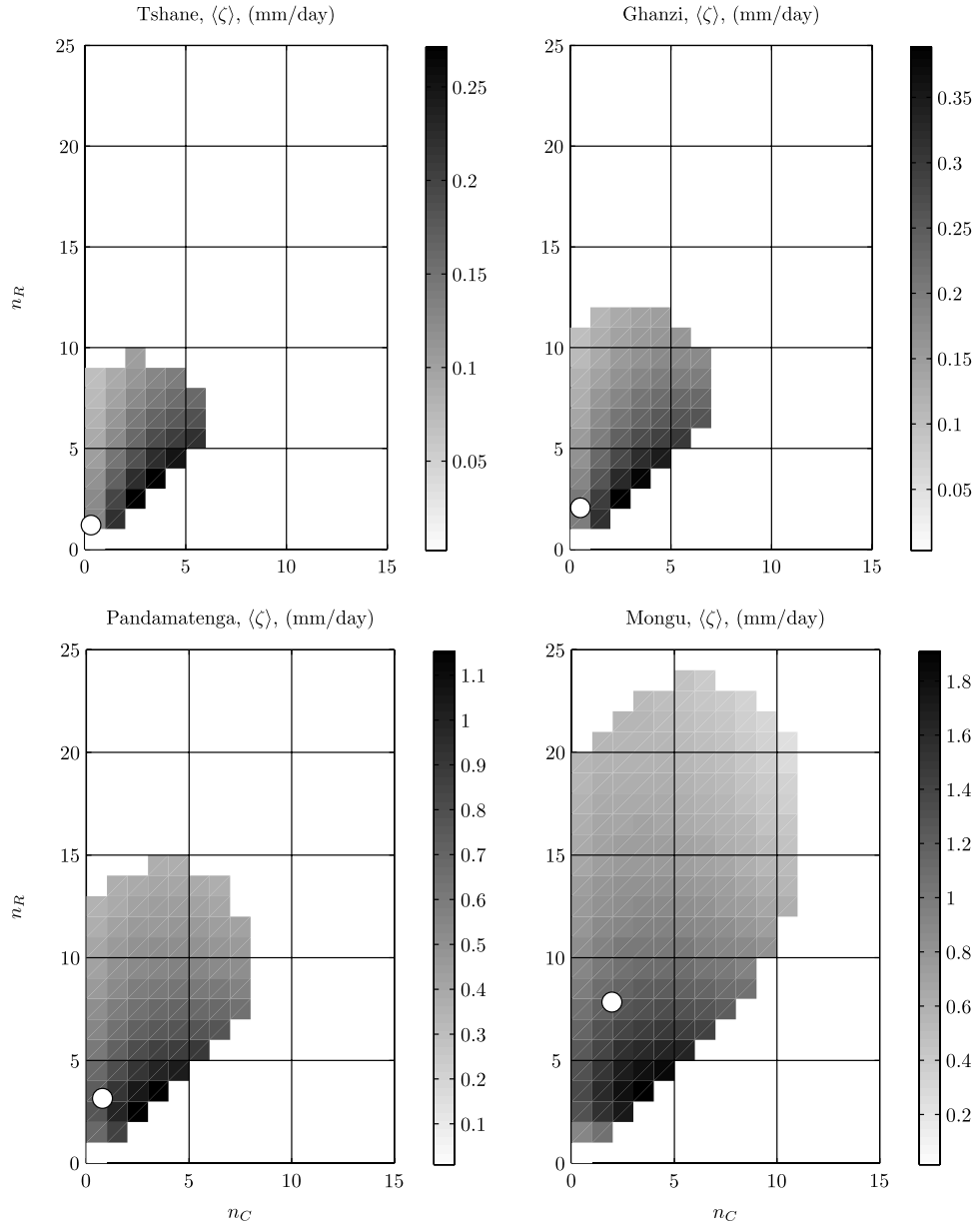

Figure 8. Model predictions of the steady state average stress-weighted plant water uptake, $\langle\zeta\rangle$, according to the number of canopies, n_C, and root systems, n_R, co-occurring within four Kalahari landscapes for all conditions where $P(n_R \cap n_C) \geq 10^{-5}$. All simulations were conducted using observed tree densities, observed average canopy size, and assuming a constant root ratio of 2 for all four landscapes. In each landscape, the maximum stress-weighted plant water uptake occurs in the same combination of roots and trees canopies, although the maximum value increases from southern landscapes (Tshane) to northern landscapes (Mongu). The point representing the landscape average number of canopies, $\langle n_C\rangle$, and roots, $\langle n_R\rangle$, is marked by an open circle in each plot.

roots cause both a significant reduction in throughfall (see equation (12)) as well as increased plant water uptake (equation (17)). At each site, the landscape average structure represents a balance between overextraction by the atmosphere and overexploitation by the vegetation, leading to minimum values of stress at these locations.

[35] Figure 8 shows the dependence of the steady state average stress-weighted plant water uptake rate, $\langle\zeta\rangle$, on the local values of n_C and n_R for each landscape. Only combinations of n_C and n_R that correspond to values of $P(n_R \cap n_C) \geq 10^{-5}$ are shown. The range of possible structures increases in northern landscapes due to the greater density and size of individual trees (Table 2). Interestingly, conditions of maximum stress-weighted plant water uptake rates occur for the same combination of root and canopy layers in each landscape. However, the magnitude of $\langle\zeta\rangle$ changes along the rainfall gradient, with the highest values occurring in more humid landscapes.

5.2. Optimal Landscape Structural Configurations

[36] We use the expression of the joint probability of n_C and n_R to calculate the landscape average value of stress-

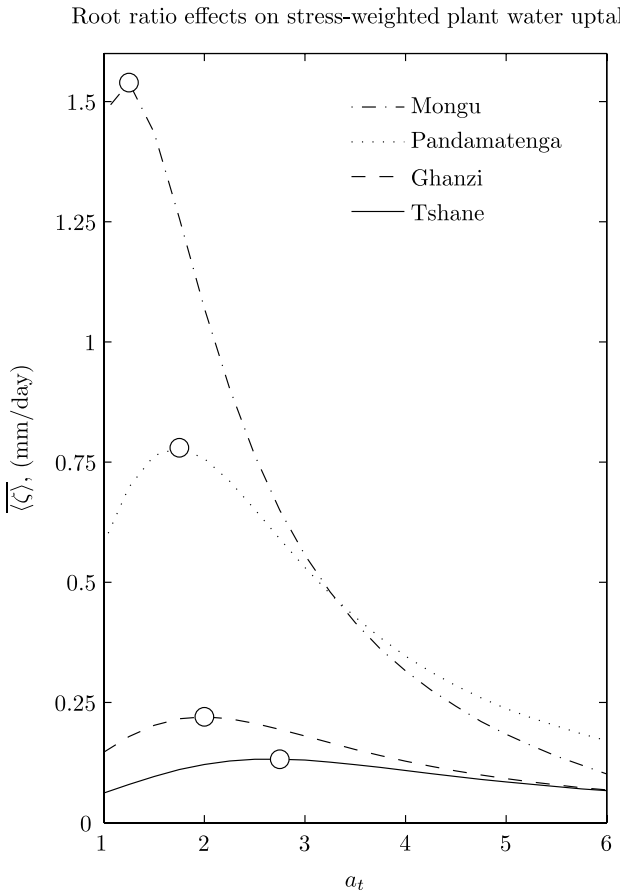

Figure 9. Effect of changing root ratio, a_t, on model predictions of the landscape-averaged distribution of stress-weighted plant water uptake, $\overline{\langle\zeta\rangle}$ (mm/d), within four Kalahari landscapes. The landscape-averaged stress-weighted plant water uptake is determined according to the product of landscape average daily plant water uptake, $\overline{\langle t\rangle}$, and the complement of the landscape average daily water stress, $(1 - \overline{\langle\xi\rangle})$ (see equation (39)). In each of the four landscapes the maximum landscape-averaged stress-weighted plant water uptake (open circle) occurs for increasingly lower values of a_t as rainfall rates increase, suggesting adaptive changes in the optimal size of lateral root extension across the rainfall gradient.

weighted plant water uptake, $\overline{\langle\zeta\rangle}$, across the Kalahari rainfall gradient. In particular, we investigate the dependence of $\overline{\langle\zeta\rangle}$ on the landscape-scale vegetation structural parameters a_t and λ_t. Figure 9 shows the relation between average stress-weighted plant water uptake and the root-to-canopy ratio, a_t. As a_t increases, both water uptake and water stress increase, due to the enhanced ability of plants to exploit the soil water resources. At a critical value of a_t for each landscape, the increase in water stress associated with larger root areas offsets the increase in plant water uptake and the value of $\overline{\langle\zeta\rangle}$ begins to decrease. This fact explains the existence of an optimal value of a_t in Figure 9 where $\overline{\langle\zeta\rangle}$ is maximum. The optimal root-to-canopy ratio, a_t, decreases with increasing values of mean annual precipitation, suggesting that sparse semiarid trees benefit from lateral root growth more than the denser woody vegetation growing in subhumid environments.

[37] Figure 10 shows the dependence of the landscape-averaged value of stress-weighted plant water uptake, $\overline{\langle\zeta\rangle}$ mm/day, on tree density, λ_t (ind/m^2). Plant water uptake increases with the tree density, while water stress initially decreases with λ_t (i.e., for low values of λ_t), due to the effect of shading on the soil water balance. As a result, an optimal value of tree density exists, which is associated with maximum stress-weighted plant water uptake. This optimal value of λ_t is found to be close to the tree densities observed in the field, suggesting that λ_t changes along the rainfall gradient to optimize the use of the water resources.

6. Conclusion

[38] Our model incorporates the effect of tree canopies and tree root systems on the local dynamics of soil moisture at a point in a landscape. We have derived the distribution of the number of intersecting canopies and root systems within

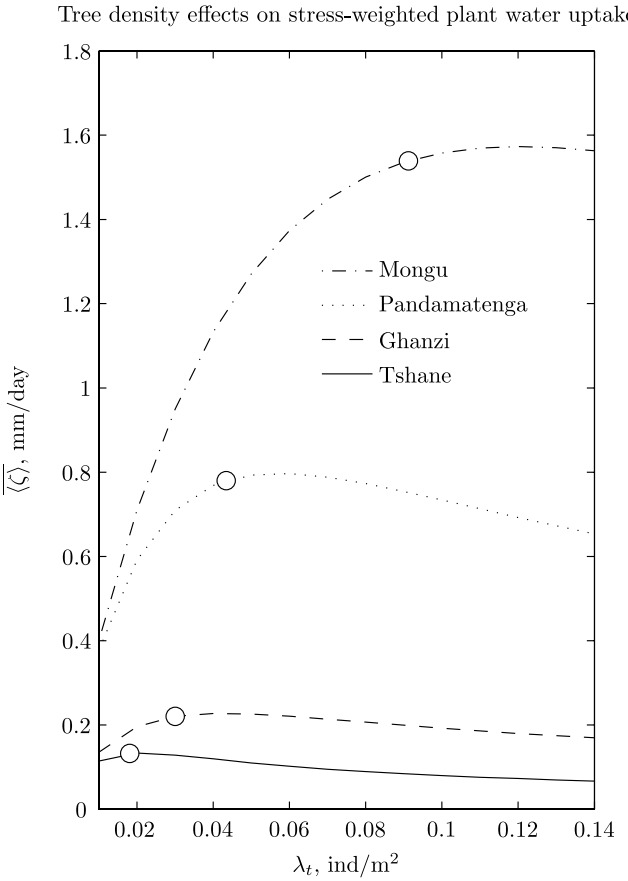

Figure 10. Effect of changing tree density, λ_t, on predictions of the landscape-averaged distribution of stress-weighted plant water uptake, $\overline{\langle\zeta\rangle}$, within four Kalahari landscapes. All simulations are conducted using the estimated optimal values of root ratio, a_t, determined from Figure 9. Open circles represent the actual density of trees from previous field observations [*Caylor et al.*, 2003] and unpublished data on Ghanzi vegetation. In each landscape the observed density of trees corresponds to a landscape-averaged stress-weighted plant water uptake that is at or just below maximum values across a wide range of possible tree densities.

a landscape based on the density of trees, the size of tree canopies and the relative size of root systems versus canopy areas. From the joint distribution of overlapping canopies and root systems, we are able to derive the distribution of mean soil moisture.

[39] This framework is used to investigate the relation between vegetation structure and the spatial dynamics of soil moisture in water-limited ecosystems. Through the application to four field sites along the Kalahari Transect, it is shown that (1) at each site, locations that contain the average vegetation structure (in terms of overlapping canopies and roots) also correspond to conditions of minimum stress, (2) there is an optimal root-to-canopy ratio that maximizes stress-weighted plant water uptake and this optimal value increases along an increasing aridity gradient, and (3) for a given root to canopy ratio, there is an optimal tree density associated with maximum stress-weighted plant water uptake. Taken as a whole, these results emphasize the important role that lateral roots play in determining the spatial patterns of soil moisture within semiarid ecosystems, as well as the need for additional data regarding changes in lateral root distribution associated with varying patterns of tree density and rainfall in water-limited ecosystems.

[40] The present work has presented a framework for connecting the distribution of individual plants to landscape-scale water balance, soil moisture dynamics, and plant water stress. We have used the model of a spatially random distribution as our starting point, but the exploration of landscape distributions of soil moisture and, more critically, plant water stress under varying nonrandom patterns of vegetation can now be permitted through the extension of the analytical approach provided here into actual observed vegetation patterns.

Appendix A: Joint Distributions of Canopy and Root Occurrences

[41] In order to derive the landscape patterns of overlapping tree and root distributions, it is necessary to know the joint distribution of root and canopy occurrences. If root systems and tree canopies were distributed randomly with respect to each other, the derivation of the joint distribution of the number of canopy and root overlappings would be prohibitively complex. However, because each tree canopy is associated with a specific root system, and the center of the individual's canopy and root system share a common location (i.e., the tree stem), it is possible to derive the joint distribution of canopy and root occurrences. For a landscape with $a_t \geq 1$, this is done using the conditional probability of the number of tree canopies occurring given a specified number of overlapping root systems, defined as $P(n_C|n_R)$ in equation (7).

[42] Before proceeding, we note the dependence of the joint distribution of roots and canopies, $P(n_R \cap n_C)$, on the conditional probability $P(n_C|n_R)$ when the specified value of a_t is greater than 1 (c.f. equation (7)). This dependence arises from the consideration that when root radii are always larger than canopy radii, the complete canopy area of each individual is entirely underlain by its corresponding root system. For this reason, it is not possible for the number of canopies occurring at a random location to exceed the number of root systems at the same location. Therefore, when $a_t \geq 1$, the number of cooccurring root systems (n_R) represents the maximum number of cooccurring canopies

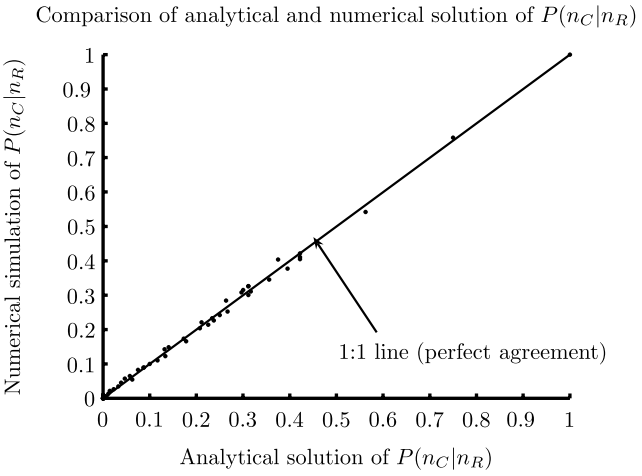

Figure A1. Comparison of numerical and analytical values of $P(n_R \cap n_C)$ for $n_C \leq 10$ and $n_R \leq 10$, when $\lambda = 0.0100$, $\mu_r = 5$ m, and $a_t = 2$.

(n_C) that can occur at each location, so for any random location in the landscape,

$$n_C \leq n_R, \qquad if\ a_t \geq 1. \tag{A1}$$

[43] The possible number of canopies that can be present at a location with n_R roots is simply $0 \ldots n_R$. In addition, for any value of n_R, it is necessary that the sum of all individual probabilities of $n_C = 0, 1, \ldots n_R$ must total 1, so that

$$\sum_{n_C=0}^{n_R} P(n_C|n_R) = 1. \tag{A2}$$

[44] Given the conditions specified in equation (A1) and equation (A2), we demonstrate the derivation of the conditional probability, $P(n_C|n_R)$, for any combination of n_R and n_C. We begin with the simplest possible scenario, which is the one arising from a location with zero root systems (i.e., $n_R = 0$). Since the number of canopies present must be less than or equal to the number of root systems present (see equation (A1)), it follows that if n_R is zero, then n_C must also be zero. Therefore we can express the conditional probability of having no canopies given the presence of no roots as $P(n_C = 0|n_R = 0) = 1$. Furthermore, the the conditional probability of having i number of canopies given the presence of no roots is $P(n_C = i|n_R = 0) = 0$ for all values of $i \neq 0$.

[45] Next, we consider the case of a random location in the landscape where only a single root system is present (i.e., $n_R = 1$). Equation (A1) specifies that when $n_R = 1$, the number of canopies present can be equal to either 0 or 1, which greatly constrains the possible scenarios we must consider. In addition, the problem is further simplified by the recognition that when $n_R = 1$ (and $a_t \geq 1$), the point under consideration is necessarily considering the root system and associated canopy area of a single individual tree. Therefore it is sufficient to determine the relative probabilities of being "not under" versus "under" an individual's canopy (i.e., $n_C = 0$ versus $n_C = 1$) given that a point is located within a single individual's root system ($n_R = 1$). These two possibilities are expressed as the probability of finding a location where only the root system is present, but no canopy is present, $P(n_C = 0|n_R = 1)$, or a

location where both the canopy area and root systems are present, $P(n_C = 1|n_R = 1)$. The probability of being in a portion of an individual's root system that is underlain by its canopy is determined by the ratio of the canopy area to root system area for each individual, which has already been defined as $1/a_t^2$. For convenience, we define $\tau = 1/a_t^2$, so that the probability of being in the portion of an individual's root system that is under its canopy, is $P(n_C = 1|n_R = 1) = \tau$. In contrast, the probability of being outside the canopy area of an individual given the presence of the individual's root system is $P(n_C = 0|n_R = 1) = (1 - \tau)$. According to equation (A2), it is required that the sum of $P(n_C = 0|n_R = 0)$ and $P(n_C = 1|n_R = 1)$ must be 1, which is met by $\tau + (1 - \tau) = 1$.

[46] Next, we examine the case of $n_R = 2$, which specifies the possible number of present canopies to be 0, 1, or 2. Because the probabilities of being under and between each of the canopy areas associated with the two overlapping root systems are independent, the probability of both canopies occurring over the pair of overlapping roots (i.e., $P(n_C = 2|n_R = 2)$) is τ^2. Similarly, the probability of neither canopy occurring, $P(n_C = 0|n_R = 2)$, is simply $(1 - \tau)^2$. However, the probability that only one canopy overlaps the two root systems is the product of the independent probabilities that one canopy is present (τ) and the other is not ($1-\tau$). Since it does not matter which canopy is present, the total conditional probability of $P(n_C = 1|n_R = 2)$ is $2(1 - \tau)\tau$. As with the case of $n_R = 1$, equation (A2) must be true so that $\tau^2 + 2(1 - \tau)\tau + (1 - \tau)^2 = 1$.

[47] Following this approach, we can define the probability of $P(n_C|n_R)$ for all possible combinations of n_R and n_C. We find that the conditional probability, $P(n_C|n_R)$, is a binomial distribution as shown in equation (8). A numerical simulation of the 2-D poisson process allows for an approximation of $P(n_R \cap n_C)$. Simulation results confirm our analytical derivation of $P(n_R \cap n_C)$, which we compare to the numerical distribution derived from a simulated poisson process. Figure A1 demonstrates the high agreement between the numerical and analytical solutions. As expected, the values of the numerical and analytical solutions of $P(n_C|n_R)$ for the range $n_C \leq 10$ and $n_R \leq 10$ plot on a 1:1 line.

[48] **Acknowledgments.** K.K.C.'s research at Princeton University was supported by a postdoctoral award from NSF's National Center for Earth-surface Dynamics (EAR-0120914) and NASA's Interdisciplinary Science Program (NASA-NNG-04-GM71G). I.R.-I. acknowledges the support of NSF through grants in Biocomplexity (DEB-0083566) and the National Center for Earth-surface Dynamics (EAR-0120914). P.D. was supported by NSF (EAR-0236621) and DOE (DEFC02-03ER63613, through NIGEC-Great Plains Regional Center).

References

Archer, S., C. Scifres, C. Bassham, and R. Maggio (1988), Autogenic succession in a subtropical savanna: Conversion of grassland to thron woodland, *Ecol. Monogr.*, *58*(2), 111–127.

Bahlotra, Y. (1987), *Climate of Botswana Part II: Elements of Climate*, Botswana Gov. Print. Off., Gaborone.

Batista, J., and D. A. Maguire (1998), Modeling the spatial structure of topical forests, *For. Ecol. Manage.*, *110*(1–3), 293–314, doi:10.1016/S0378-1127(98)00296-5.

Bonan, G. B., and H. H. Shugart (1989), Environmental factors and ecological processes in boreal forests, *Annu. Rev. Ecol. Syst.*, *20*, 1–28.

Breshears, D. D., and F. J. Barnes (1999), Interrelationships between plant functional types and soil moisture heterogeneity for semiarid landscapes within the grassland/forest continuum: A unified conceptual model, *Landscape Ecol.*, *14*(5), 465–478, doi:10.1023/A:1008040327508.

Brutsaert, W. (1982), *Evaporation Into the Atmosphere*, Springer, New York.

Caylor, K. K., H. H. Shugart, P. R. Dowty, and T. M. Smith (2003), Tree spacing along the Kalahari transect in southern Africa, *J. Arid Environ.*, *54*(2), 281–296, doi:10.1006/jare.2002.1090.

Cox, D., and H. Miller (1965), *The Theory of Stochastic Processess*, Methuen, London.

Denslow, J. S. (1987), Tropical rainforest gaps and tree species diversity, *Annu. Rev. Ecol. Syst.*, *18*, 431–451.

Hipondoka, M. H. T., J. N. Aranibar, C. Chirara, M. Lihavha, and S. A. Macko (2003), Vertical distribution of grass and tree roots in arid ecosystems of southern Africa: Niche differentiation or competition?, *J. Arid Environ.*, *54*(2), 319–325, doi:10.1006/jare.2002.1093.

Huxman, T. E., B. P. Wilcox, D. D. Breshears, R. L. Scott, K. A. Snyder, E. E. Small, K. Hultine, W. T. Pockman, and R. B. Jackson (2005), Ecohydrological implications of woody plant encroachment, *Ecology*, *86*(2), 308–319.

Jeltsch, F., K. Moloney, and S. J. Milton (1999), Detecting process from snapshot pattern: Lessons from tree spacing in the southern Kalahari, *Oikos*, *85*(3), 451–466.

Laio, F., A. Porporato, L. Ridolfi, and I. Rodriguez-Iturbe (2001), Plants in water-controlled ecosystems: Active role in hydrologic processes and response to water stress—II. Probabilistic soil moisture dynamics, *Adv. Water Resour.*, *24*(7), 707–723, doi:10.1016/S0309-1708(01)00005-7.

Ludwig, J. A., B. P. Wilcox, D. D. Breshears, D. J. Tongway, and A. C. Imeson (2005), Vegetation patches and runoff-erosion as interacting ecohydrological processes in semiarid landscapes, *Ecology*, *86*(2), 288–297.

Porporato, A., F. Laio, L. Ridolfi, and I. Rodriguez-Iturbe (2001), Plants in water-controlled ecosystems: Active role in hydrologic processes and response to water stress—III. Vegetation water stress, *Adv. Water Resour.*, *24*(7), 725–744, doi:10.1016/S0309-1708(01)00006-9.

Porporato, A., F. Laio, L. Ridolfi, K. Caylor, and I. Rodriguez-Iturbe (2003), Soil moisture and plant stress dynamics along the Kalahari precipitation gradient, *J. Geophys. Res.*, *108*(D3), 4127, doi:10.1029/2002JD002448.

Rodriguez-Iturbe, I., P. D'Odorico, A. Porporato, and L. Ridolfi (1999a), On the spatial and temporal links between vegetation, climate, and soil moisture, *Water Resour. Res.*, *35*(12), 3709–3722.

Rodriguez-Iturbe, I., A. Porporato, L. Ridolfi, V. Isham, and D. R. Cox (1999b), Probabilistic modelling of water balance at a point: The role of climate, soil and vegetation, *Proc. R. Soc. London, Ser. A*, *455*, 3789–3805.

Runkle, J. R., and T. C. Yetter (1987), Treefalls revisited: Gap dynamics in the southern Appalachians, *Ecology*, *68*(2), 417–424.

Sankaran, M., et al. (2005), Determinants of woody cover in African savannas: A continental scale analysis, *Nature*, *438*, 846–849, doi:10.1038/nature04070.

Scholes, R., and B. Walker (1993), *An African Savanna: Synthesis of the Nylsvley Study*, Cambridge Univ. Press, New York.

Scholes, R. J., P. R. Dowty, K. Caylor, D. A. B. Parsons, P. G. H. Frost, and H. H. Shugart (2002), Trends in savanna structure and composition along an aridity gradient in the Kalahari, *J. Veg. Sci.*, *13*(3), 419–428.

Seyfried, M. S., S. Schwinning, M. A. Walvoord, W. T. Pockman, B. D. Newman, R. B. Jackson, and E. M. Phillips (2005), Ecohydrological control of deep drainage in arid and semiarid regions, *Ecology*, *86*(2), 277–287.

Shugart, H. (1984), *A Theory of Forest Dynamics*, Springer, New York.

Thomas, D. S., and P. A. Shaw (1991), *The Kalahari Environment*, Cambridge Univ. Press, New York.

Tilman, D. (1988), *Plant Strategies and the Dynamics and Structure of Plant Communities*, *Monogr. Popul. Biol.*, vol. 26, Princeton Univ. Press, Princeton, N. J.

Tilman, D., and P. M. Kareiva (1997), *Spatial Ecology: The Role of Space in Population Dynamics and Interspecific Interactions*, *Monogr. Popul. Biol.*, vol. 30, Princeton Univ. Press, Princeton, N. J.

Williams, C. A., and J. D. Albertson (2004), Soil moisture controls on canopy-scale water and carbon fluxes in an African savanna, *Water Resour. Res.*, *40*, W09302, doi:10.1029/2004WR003208.

K. K. Caylor, Department of Geography, Indiana University, 701 East Kirkwood Avenue, Bloomington, IN 47405, USA. (caylor@indiana.edu)

P. D'Odorico, Department of Environmental Sciences, University of Virginia, 291 McCormick Road, Box 400123, Charlottesville, VA 22904-4123, USA.

I. Rodriguez-Iturbe, Department of Civil and Environmental Engineering, Princeton University, E-220 Engineering Quad, Princeton, NJ 08544, USA.